Behavioral/Systems/Cognitive

Two Slow Calcium-Activated Afterhyperpolarization Currents Control Burst Firing Dynamics in Gonadotropin-Releasing Hormone Neurons

Kiho Lee (이기호),[1] Wen Duan (段文),[2] James Sneyd,[2] and Allan E. Herbison[1]

[1]Centre for Neuroendocrinology and Department of Physiology, University of Otago, Dunedin 9054, New Zealand, and [2]Department of Mathematics, University of Auckland, Auckland 1142, New Zealand

Gonadotropin-releasing hormone (GnRH) neurons release GnRH in a pulsatile manner to control fertility in all mammals. The mechanisms underlying burst firing in GnRH neurons, thought to contribute to pulsatile GnRH release, are not yet understood. Using minimally invasive, dual electrical– calcium recordings in acute brain slices from GnRH-Pericam transgenic mice, we find that the soma/proximal dendrites of GnRH neurons exhibit long-duration (~10 s) calcium transients that are perfectly synchronized with their burst firing. These transients were found to be generated by calcium entry through voltage-dependent L-type calcium channels that was amplified by inositol-1,4,5-trisphosphate receptor-dependent store mechanisms. Perforated-patch current- and voltage-clamp electrophysiology coupled with mathematical modeling approaches revealed that these broad calcium transients act to control two slow afterhyperpolarization currents (sI_{AHP}) in GnRH neurons: a quick-activating apamin-sensitive sI_{AHP} that regulates both intraburst and interburst dynamics, and a slow-onset UCL2077-sensitive sI_{AHP} that regulates only interburst dynamics. These observations highlight a unique interplay between electrical activity, calcium dynamics, and multiple calcium-regulated sI_{AHP}s critical for shaping GnRH neuron burst firing.

Introduction

Calcium entry following the action potential has multiple effects on neuronal behavior including the activation of hyperpolarizing potassium channels that help shape the action potential and subsequent firing of the neuron (Berridge, 1998). Traditionally, these afterhyperpolarizations (AHPs) have been divided into fast (fAHP), medium (mAHP), and slow (sAHP) components mediated principally by large-conductance (BK; $K_{Ca}1.1$), small-conductance (SK; $K_{Ca}2.1$–2.3) and molecularly uncharacterized Ca^{2+}-activated potassium channels, respectively (Sah and Faber, 2002; Vogalis et al., 2003; Maylie et al., 2004; Pedarzani and Stocker, 2008). The BK channel, with a decay of <50 ms, contributes to repolarization of the action potential (Salkoff et al., 2006), whereas the predominantly SK-mediated mAHP, typically with a decay of several hundred ms, controls spike discharge frequency (Sah and Faber, 2002; Pedarzani and Stocker, 2008). The precise identity of channels underlying the sAHP have remained enigmatic but their slow decay kinetics, in the order of seconds, have made them attractive targets for regulating spike frequency adaptation (SFA) and rhythmic firing patterns (Nicoll, 1988; Sah and Faber, 2002; Goldberg and Wilson, 2005; Wilson and Goldberg, 2006). It is increasingly apparent that individual neuronal phenotypes use different combinations of Ca^{2+}-dependent potassium channels to generate their AHP and firing characteristics (Yamada et al., 2004; Power and Sah, 2008).

The gonadotropin-releasing hormone (GnRH) neurons represent the final output cells of the neuronal network controlling fertility in mammals. The cell bodies of these neurons are dispersed within the basal forebrain but project axons to a tightly circumscribed area in the basal hypothalamus, from which they release GnRH in an episodic manner. This drives pulsatile gonadotropin secretion from the pituitary gland that is essential for gonadal function (Herbison, 2006). Although the mechanisms driving GnRH neuron burst firing remain unknown, it is likely that, taking inference from other neuroendocrine cell types, the generation of bursting patterns of electrical activity in GnRH neurons underlie episodic GnRH release (Leng and Brown, 1997; Moenter et al., 2003; Herbison, 2006).

We recently generated a transgenic mouse line in which the genetically encodable Pericam Ca^{2+} indicator (Nagai et al., 2001) was targeted selectively to GnRH neurons (Jasoni et al., 2007). Real-time imaging of intracellular Ca^{2+} concentration ($[Ca^{2+}]_i$) in adult GnRH neurons in acute brain slices from these mice revealed a subpopulation of neurons exhibiting spontaneous long-duration (~10 s) Ca^{2+} transients, a phenomenon not previously reported in the mature brain (Jasoni et al., 2007). Using noninvasive dual electrical recording–Ca^{2+} imaging approaches we find here that these Ca^{2+} transients occur only in burst firing GnRH neurons and result from voltage-dependent membrane Ca^{2+} entry amplified by Ca^{2+}-induced Ca^{2+} release from inositol-1,4,5-trisphosphate receptor (IP_3R)-dependent stores.

Received Dec. 4, 2009; revised Feb. 10, 2010; accepted Feb. 22, 2010.

These studies were supported by the New Zealand Marsden Fund and Health Research Council.

Correspondence should be addressed to Allan E. Herbison, Centre for Neuroendocrinology, Department of Physiology, University of Otago School of Medical Sciences, P.O. Box 913, Dunedin 9054, New Zealand. E-mail: allan.herbison@stonebow.otago.ac.nz.

DOI:10.1523/JNEUROSCI.6156-09.2010

 0270-6474/10/306214-11$15.00/0

Electrophysiological and modeling approaches revealed the presence of large calcium-activated (~20 s) AHPs in GnRH neurons generated by fast activating, long-duration apamin-sensitive channels and slow activating, long-duration UCL2077 (Shah et al., 2006)-sensitive channels. These two channels had distinct roles in regulating GnRH neuron burst firing with the apamin-sensitive sI_{AHP} controlling both the structure of firing within bursts and interburst interval (IBI) while UCL-sensitive sI_{AHP} determined solely interburst dynamics.

Materials and Methods

Animals and slice preparation. Adult (6–12 weeks old, male or female) homozygous GnRH-Pericam (Jasoni et al., 2007) and GnRH-GFP (Spergel et al., 1999) transgenic mice were used for all studies and housed according to standard laboratory conditions. The University of Otago Animal Ethics Committee approved all experimentation. Brain slices were prepared as reported previously (Han et al., 2005; Jasoni et al., 2007). In brief, mice were killed between 09:00–12:00 h, brains quickly dissected and cut on a vibratome into 200-μm-thick coronal slices containing the rostral preoptic area, and maintained in oxygenated artificial CSF (ACSF) containing the following (in mM): 118 NaCl, 3 KCl, 2.5 $CaCl_2$, 1.2 $MgCl_2$, 5 HEPES, 25 $NaHCO_3$, 11 D-glucose, pH 7.3, 300~310 mOsm, at 30°C for at least 60 min before imaging. Slices were then placed on the stage of an Olympus BX51 upright microscope equipped with a slice chamber and perfused with oxygenated ACSF solution at a rate of 3–4 ml/min. Recordings were undertaken at room temperature (21−23°C) unless indicated otherwise.

Dual Ca^{2+}–electrical recordings. The electrical properties and firing behavior of individual GnRH neurons are identical in GnRH-Pericam and GnRH-EGFP transgenic mice (K. Lee and A. E. Herbison, unpublished data). $[Ca^{2+}]_i$ was monitored in individual GnRH neurons as reported previously (Jasoni et al., 2007; Romanò et al., 2008) with slight modifications. In brief, excitation was performed by exposing slices to 415 nm wavelength for 100 ms every second using Sutter λ DG-4 high-speed filter unit. Images were filtered at 525 nm and acquired using Metafluor 7.1 software to control the DG-4 and liquid-cooled ORCA-ER CCD camera (Hamamatsu) unit. Fluorescence intensities of emitted light from both a region of interest on the soma and the same area from the background were exported and analyzed with Origin Pro 7.5 to calculate the change of the intracellular calcium concentration. Calcium transients are presented as follows: $[Ca^{2+}]_i = [F(t) - F_{rest}(t)]/F_{rest}(t)$, where $F(t)$ and $F_{rest}(t)$ represent the soma and the background fluorescence intensity at time t, respectively. Values were then normalized into a percentage scale against $[Ca^{2+}]_i$ at starting time. Cell-attached recordings of action currents (representing action potentials) from GnRH-Pericam neurons were made using glass pipettes (outer diameter: 1.5 mm; inner diameter: 1.17; tip resistance 5–7 MΩ) filled with 140 mM NaCl solution (Perkins, 2006). By applying a slight suction onto the cell membrane of Pericam-positive GnRH neurons, a loose seal (20–30 MΩ) was formed and recordings undertaken with a Multiclamp 700A amplifier (Molecular Devices) and Clampex 10.2 software. Action current signals (50–400 pA amplitude) were sampled at 1 kHz speed and filtered at 10 kHz with a Bessel filter. Electrical and Ca^{2+} recordings were synchronized by using Metafluor to control pClamp.

Perforated-patch-clamp recordings. Gramicidin-perforated-patch recordings of GnRH neurons were undertaken as reported previously (Han et at 2005). In brief, adult male GnRH-EGFP mice were decapitated and 200-μm-thick coronal slices containing the rostral preoptic area prepared in a same way used for slice preparation from GnRH-Pericam mice. Slices were viewed with a fixed-stage upright microscope (BX51WI, Olympus) and either fluorescence illumination, using the reflected light fluorescence illuminator (BX-RFA, Olympus) and filter (U-MWIBA2, BA510–550, Olympus), or Nomarski differential interference contrast optics. Gramicidin (Sigma) was dissolved in dimethylsulfoxide (Sigma) to a concentration of 10 mg/ml and then diluted in the pipette solution [containing the following (in mM): 135 K-gluconate, 5 NaCl, 1 $CaCl_2$, 1 $MgCl_2$, 10 HEPES, 0.2 EGTA, 5 MgATP, 0.1 Na_2GTP, pH 7.3, 286 mOsm] to a final concentration of 30–60 μg/ml just before use and sonicated for 2–3 min. Following formation of tight gigaohm seal, access resistance was monitored at regular intervals and experiments undertaken when access resistance had stabilized (10–30 min) between 30 and 100 MΩ. The patch configuration typically went into "whole-cell" mode when access resistance fell below 20 MΩ. Perforated-patch-clamp recordings were performed using a Multiclamp 700A. The tip resistance of the electrodes was 4–7 MΩ. Signals were sampled online using a Digidata 1322A interface (Molecular Devices) connected to a PC. Signals were filtered (10 kHz, Bessel filter of Multiclamp 700A) before digitizing at a rate of 1 kHz. Acquisition and subsequent analysis of the acquired data were performed using the Clampex 10.2 suite of software (Molecular Devices). Calculated junction potential of 14.8 mV was adjusted. Pipette capacitance and membrane capacitance were compensated.

Treatments. All drugs (Tocris Biosciences) were applied to the ACSF bathing solution at the following established concentrations: apamin 300 nM (Liu and Herbison, 2008), UCL2077 10 μM (Shah et al., 2006), 2-aminoethoxydiphenylborate (2-APB) 100 μM (Jasoni et al., 2007), cyclopiazonic acid (CPA) 30 μM (Power and Sah, 2008) and tetrodotoxin (TTX) 0.5 μM (Sim et al., 2001). Apamin and TTX were dissolved in water while the others were dissolved initially in dimethylsulfoxide resulting in a final dimethylsulfoxide concentration in the perfusion solution of 0.03 to 0.1%.

Statistical analysis. Correlation between single dependent and multiple independent variables was assessed with multiple regression method. Differences between the means were tested by Wilcoxon signed-ranks test unless indicated otherwise. Data are presented as mean ± SEM.

Mathematical model of GnRH neuron calcium dynamics and electrical activity. The equation for membrane potential (V) is given by the following:

$$C_m \frac{dV}{dt} = -I_{ionic}(V,t) + I_{inj}, \quad (1)$$

where C_m is the membrane capacitance, I_{inj} represents a stochastically modeled synaptic injection current and $I_{ionic} = I_{naf} + I_{nap} + I_{kdr} + I_{kir} + I_{km} + I_{cal} + I_{cat} + sI_{AHP\text{-}SK} + sI_{AHP\text{-}UCL} + I_{leak}$.

I_{naf} represents the fast sodium current; I_{nap} a persistent sodium current; I_{kdr}, I_{kir}, and I_{km} denote delayed rectifier, inward rectifier, and M-type potassium currents, respectively; I_{cal} and I_{cat} are L- and T-type calcium currents, respectively. Equations for these currents are taken from LeBeau et al. (2000) and Roberts et al. (2009). The two pacemaker currents are an SK-type $[Ca^{2+}]_i$-activated K^+ current ($sI_{AHP\text{-}SK}$), and a slow $[Ca^{2+}]_i$-activated afterhyperpolarization current ($sI_{AHP\text{-}UCL}$). I_{leak} is the passive membrane leakage current.

Conventional Hodgkin–Huxley-type models are used for all currents, as follows:

$$I_{naf} = g_{naf} M_{naf\infty}^3 H_{naf} (V - V_{na}), \quad (2)$$

$$I_{kdr} = g_{kdr} N_{kdr}^4 (V - V_k), \quad (3)$$

$$I_{kir} = g_{kir} N_{kir\infty} (V - V_k), \quad (4)$$

$$I_{km} = g_{km} N_{km} (V - V_k), \quad (5)$$

$$I_{cal} = g_{cal} M_{cal\infty}^2 (V - V_{ca}), \quad (6)$$

$$I_{cat} = g_{cat} M_{cat\infty}^2 H_{cat\infty} (V - V_{ca}), \quad (7)$$

$$I_{nap} = g_{nap} M_{nap\infty}^3 H_{nap\infty} (V - V_{na}), \quad (8)$$

and

$$sI_{AHP\text{-}SK} = g_{sk} \left(\frac{c^{n_{sk}}}{c^{n_{sk}} + K_{sk}^{n_{sk}}} \right) (V - V_k), \quad (9)$$

where c is the cytoplasmic concentration of free intracellular calcium. Equations for N_{kdr} and N_{km}, or H_{naf} have the following form:

$$\frac{dx}{dt} = \frac{x_\infty - x}{\tau_x}, \quad (10)$$

while all other gating variables are set to their steady-state values. The steady-state functions are as follows:

$$M_{naf_\infty} = (1 + \exp(-(V + 40)/4.3))^{-1}, \quad (11)$$

$$H_{naf_\infty} = (1 + \exp(-(V + 66.1)/10.8))^{-1}, \quad (12)$$

$$M_{nap_\infty} = (1 + \exp(-(V + 70)/4.1))^{-1}, \quad (13)$$

$$H_{nap_\infty} = (1 + \exp(-(V + 80)/5))^{-1}, \quad (14)$$

$$N_{kdr_\infty} = (1 + \exp(-(V + 25)/15))^{-1}, \quad (15)$$

$$N_{kir_\infty} = 0.8(1 + \exp(-(V + 80)/12))^{-1} + 0.2, \quad (16)$$

$$N_{km_\infty} = (1 + \exp(-(V + 37)/4))^{-1}, \quad (17)$$

$$M_{cal_\infty} = (1 + \exp(-(V + 30)/2))^{-1}, \quad (18)$$

$$M_{cat_\infty} = (1 + \exp(-(V + 56.1)/10))^{-1}, \quad (19)$$

and

$$H_{cat_\infty} = (1 + \exp(-(V + 86.4)/4.7))^{-1}. \quad (20)$$

The time constants τ_x (units in milliseconds) are as follows:

$$\tau_{H_{naf}} = 75/(\exp((V + 80)/19) + 2\exp(-2(V + 80)/19)), \quad (21)$$

$$\tau_{N_{kdr}} = 21/(\exp((V + 30)/15) + \exp(-(V + 30)/15)) + 1.4, \quad (22)$$

and

$$\tau_{N_{km}} = 16/(\exp((V + 30)/15) + \exp(-(V + 30)/15)). \quad (23)$$

The equation for sI_{AHP}-UCL is as follows:

$$sI_{AHP\text{-}UCL} = g_{UCL}(O_{UCL} + O^*_{UCL})(V - V_k). \quad (24)$$

The following reaction scheme governs the sI_{AHP}-UCL subunit transitions:

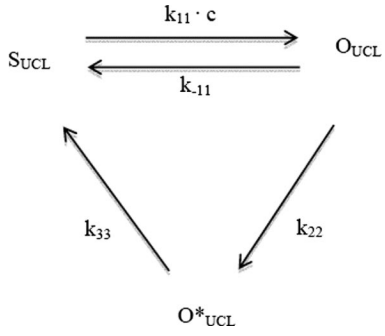

where O_{UCL} and O^*_{UCL} are two open states and S_{UCL} is the closed state.

The equation for I_{leak} is as follows:

$$I_{leak} = g_{leak}(V - V_{leak}). \quad (25)$$

The equations governing Ca^{2+} handling are as follows:

$$\frac{dc}{dt} = \rho(J_{in} - J_{pm}) + J_{release} - J_{SERCA} \quad (26)$$

and

$$\frac{dc_e}{dt} = \gamma(J_{SERCA} - J_{release}), \quad (27)$$

Table 1. Parameter values for mathematical model

Parameter	Value	Parameter	Value
C_m	16 pF	g_{naf}	190 nS
g_{nap}	20 nS	g_{kdr}	2 nS
g_{kir}	0.02 nS	g_{km}	8 nS
g_{cal}	0.05 nS	g_{cat}	2.1 nS
g_{sk}	0.3 nS	g_{UCL}	950 nS
g_{leak}	0.0389 nS	V_{na}	60 mV
V_k	−80 mV	V_{ca}	100 mV
V_{leak}	100 mV	k_{11}	1×10^{-7}
k_{-11}	1.2	k_{22}	0.5
k_{33}	3×10^{-5}	K_{sk}	1 μM
n_{sk}	2	a_1	1×10^{-4}
a_2	35 ms	a_3	300 ms
a_4	7 ms	a_5	35 ms
α	4.8×10^{-3} μM · μM · ms^{-1} · pA^{-1}	J_{er}	4×10^{-7} ms^{-1}
K_f	1.92×10^{-4} ms^{-1}	V_{NaCa}	3.5×10^{-4} μM · ms^{-1}
V_p	4.2×10^{-3} μM · ms^{-1}	K_p	0.425 s
γ	27	K_{NaCa}	0.05 s
β	2×10^{-5} ms	P_{rate}	1
IP_3	0.3 μM	ρ	0.5
$\delta 1$	1×10^{-9}	$\delta 2$	1×10^{-8}

where c is the cytoplasmic free calcium concentration, and c_e is the concentration of calcium in the endoplasmic reticulum (ER) (Li et al., 1994; Keener and Sneyd, 2008). The individual Ca^{2+} flux terms are as follows:

$$J_{in} = -\alpha(I_{cal} + I_{cat}) + \beta \cdot IP_3$$

(influx across the plasma membrane), (28)

$$J_{pm} = V_p \frac{c^2}{c^2 + K_p^2} + V_{NaCa} \frac{c^4}{c^4 + K_{NaCa}^4}$$

(efflux across the plasma membrane), (29)

$$J_{SERCA} = P_{rate} \frac{c - a_1 c_e}{a_2 + a_3 c + a_4 c_e + a_5 c c_e}$$

(ATPase pumping into the ER), (30)

and

$$J_{release} = (K_f P_o + J_{er})(c_e - c),$$

[efflux from the ER through the IP3 receptor (IP3R)]. (31)

To model the IPR, we used the study by Sneyd and Dufour (2002).

The voltage submodel affects the calcium submodel via two calcium currents (I_{cal} and I_{cat}) which act as inputs to the calcium submodel. On the other hand, cytosolic calcium affects the voltage submodel via the calcium dependence of $sI_{AHP\text{-}SK}$ and $sI_{AHP\text{-}UCL}$. Parameter values for the voltage submodel are (mostly) taken from LeBeau et al. (2000) and Roberts et al. (2009). The exceptions are the rate constants in the Markov model of the $sI_{AHP\text{-}UCL}$ current. These parameters were chosen so as to predict the correct IBI. All the parameter values for the calcium submodel are taken from previous work and are shown in Table 1 (Sneyd and Dufour, 2002; Keener and Sneyd, 2008).

I_{inj} is set as a uniform distribution from 0.02 to 0.08 pA. Wiener processes are applied on variables O_{UCL} and O^*_{UCL} with noise SDs of $\delta 1$ and $\delta 2$, respectively. These values were chosen by trial and error so as to obtain approximately correct bursting statistics. However, no detailed fit to the statistics was done.

Results

The GnRH-Pericam transgenic mouse has the advantage of enabling real-time measurement of $[Ca^{2+}]_i$ in the soma and prox-

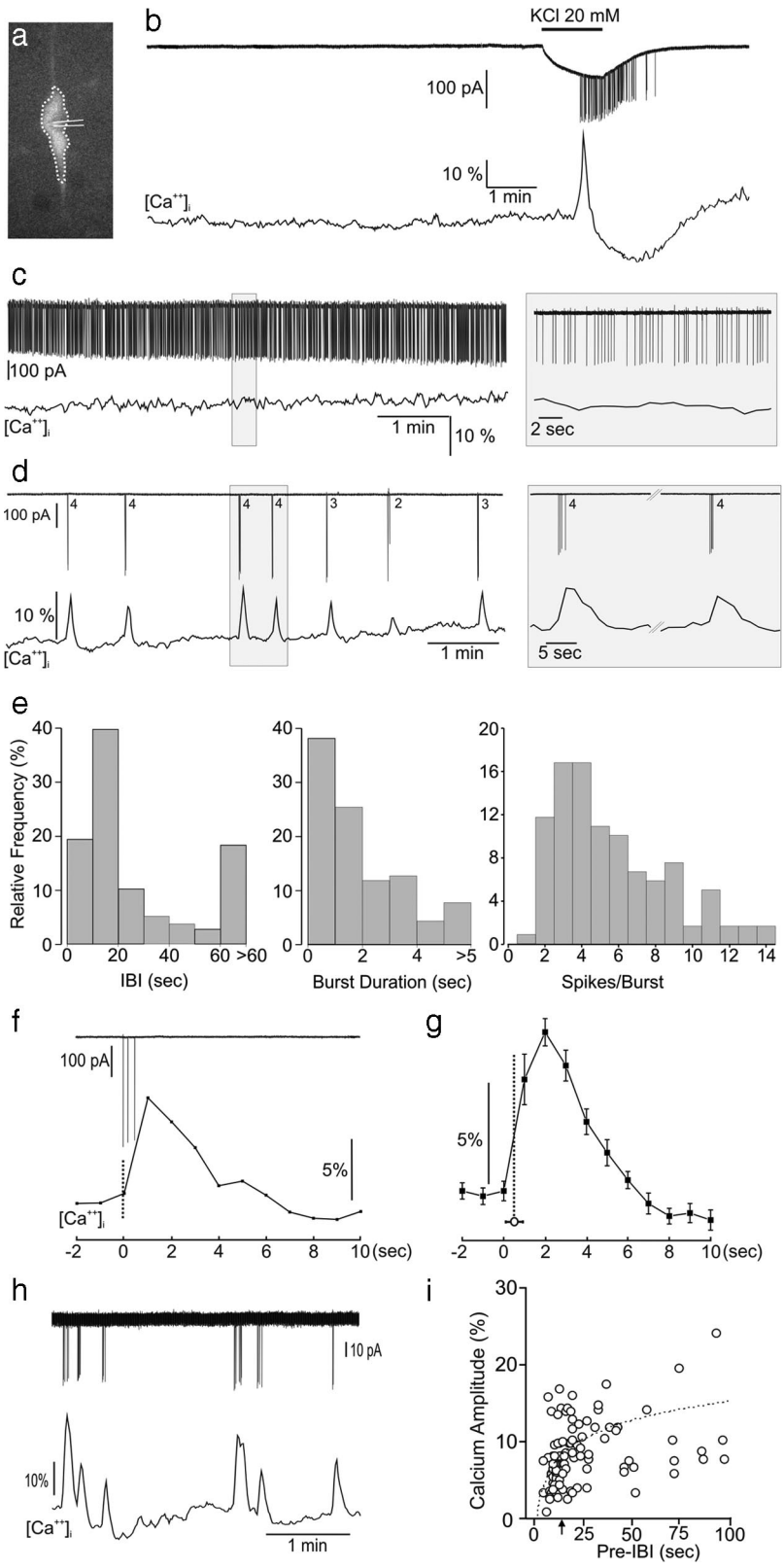

Figure 1. Relationship between action potential spiking and intracellular calcium concentrations $[Ca^{2+}]_i$ in adult GnRH neurons. ***a***, Fluorescent GnRH neuron in a brain slice of a GnRH-Pericam transgenic mouse indicating the soma/proximal dendrite area of interest (dotted line) for $[Ca^{2+}]_i$ imaging and cell-attached recording electrode. ***b***, Real-time dual electrical (action currents; top)–Ca^{2+} (bottom) recording from a silent GnRH neuron subsequently challenged with 20 mM KCl that generates a burst of firing and associated Ca^{2+} transient. ***c***, Dual recording from a continuously active GnRH neuron. ***d***, Dual recording from a burst firing GnRH neuron showing the typical perfect correlation between each burst (numbers = number spikes in burst) and occurrence of Ca^{2+} transients. ***e***, Parameters of burst firing in GnRH neurons, IBI. ***f***, Higher-temporal-resolution view of relationship between a three-spike burst and Ca^{2+} transient. ***g***, Average of burst-transient timing by setting Ca^{2+} datum point immediately before the transient rise (defined as $3 \times$ SD) as $t = 0$ and determining the time between that and the initiation of the burst (mean ± SEM; vertical dotted line). ***h***, ***i***, A significant correlation existed between IBI and the amplitude of the subsequent Ca^{2+} transient ($r = 0.49$, $p < 0.001$, $n = 106$; Spearman rank correlation) with transients occurring within ~15 s (arrow) of the last burst having reduced amplitudes.

imal dendrites of GnRH neurons *in situ* (Fig. 1*a*) without requiring loading of the cells or altering their internal milieu. The ratiometric Pericam exhibits a monophasic Ca^{2+} dependence with a dissociation constant (K_d) of 1.7 μM and Hill constant of 1.1 (Nagai et al., 2001). Initially, we performed minimally invasive loose-cell patch to make dual recordings of $[Ca^{2+}]_i$ and action currents from adult GnRH neurons in the acute brain slice preparation. Recordings made for a minimum of 10 min from 217 adult (6–12 weeks old) GnRH neurons (56 male, 161 diestrous female) revealed three types of $[Ca^{2+}]_i$-firing relationships. The first (41%) comprised of "silent" GnRH neurons that had no action currents and exhibited a flat $[Ca^{2+}]_i$ profile (Fig. 1*b*). When challenged with 20 mM potassium, silent GnRH neurons became active firing a train of action potentials that was associated with the generation of a Ca^{2+} transient followed by a subsequent depression in $[Ca^{2+}]_i$ (Fig. 1*b*). The second type of cell was tonically active firing at a relatively constant rate (mean 2.6 ± 0.3 Hz, range 1.0–3.5 Hz) but was rare ($n = 7$, 3%) and displayed a flat $[Ca^{2+}]_i$ profile (Fig. 1*c*). The final subpopulation (56%) of GnRH neurons exhibited burst firing for which there was perfect one-to-one correlation between bursts and Ca^{2+} transients (Fig. 1*d*). No differences in the percentages of the three different populations were found between male and female mice.

The relationship between burst firing and $[Ca^{2+}]_i$ profile was evaluated in detail by analyzing 119 bursts from 13 randomly selected burst firing GnRH neurons. Analyses of GnRH neuron burst firing revealed a mean (±SEM) IBI of 40 ± 6 s, but with a bimodal-type distribution (Fig. 1*e*), mean burst duration of 2.2 ± 0.2 s with 90% of bursts being shorter than 5 s (Fig. 1*e*), mean spikes per burst of 5.7 ± 0.3 with 90% bursts having <10 spikes (Fig. 1*e*), and a mean interspike interval of 497 ± 51 ms. The associated Ca^{2+} transients had a mean T_{rise} (baseline +10% to peak maximum) of 3.1 ± 0.2 s, T_{decay} (peak maximum to decay baseline + 10%) of 5.1 ± 0.2 s, duration of 8.2 ±

0.4 s, and amplitude of 10.4 ± 0.7% baseline (Fig. 1*f*,*g*). Although limited by the 1 Hz $[Ca^{2+}]_i$ imaging resolution, temporal correlations between burst onset and calcium onset indicated that Ca^{2+} transients followed burst initiation (Fig. 1*f*,*g*). Multiple regression analysis between the five burst parameters and three calcium parameters (T_{rise}, T_{decay}, amplitude) revealed only two significant associations: (1) T_{decay} was positively associated with burst duration ($\beta = 0.66$, adjusted r2 = 0.50, $p < 0.01$) and (2) Ca^{2+} amplitude was associated with the pre-IBI ($\beta = 0.60$, adjusted r2 = 0.44, $p < 0.01$) such that an IBI of <15 s resulted in a transient with reduced amplitude (Fig. 1*i*), also observed in the raw traces (Fig. 1*h*). These results show that, as long as bursts arise with an interval of >15 s, Ca^{2+} transients of normal amplitude occur and greatly outlast the duration of the burst.

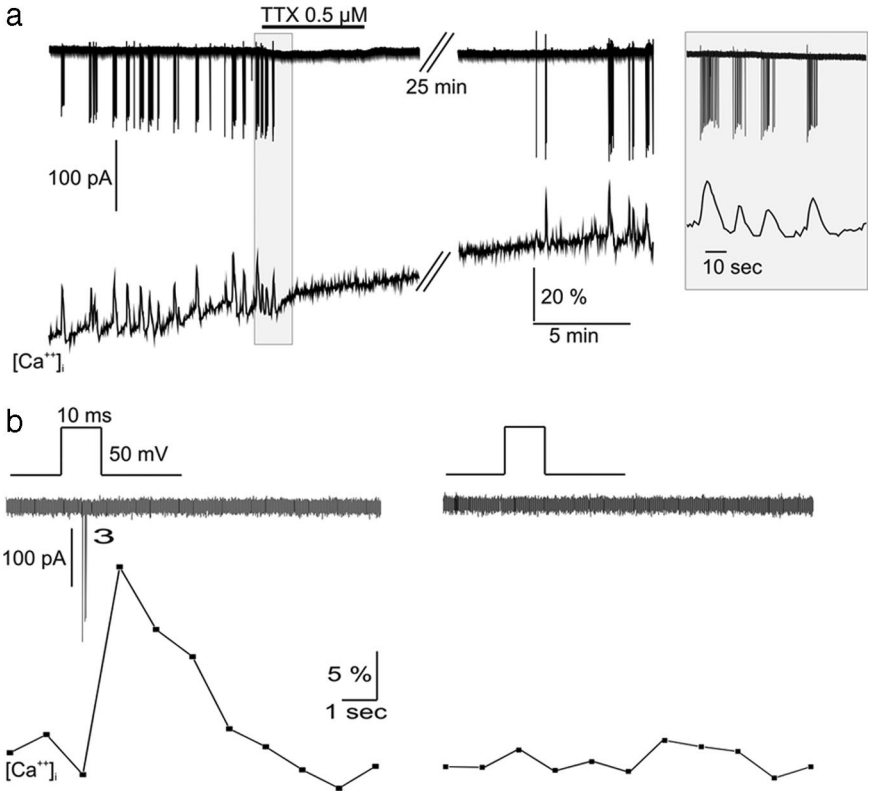

Figure 2. Burst firing drives calcium transients in GnRH neurons. ***a***, Blocking voltage-dependent sodium channels with TTX stops both action potential firing and Ca^{2+} transients. ***b***, Electrical stimulation applied through the cell-attached patch electrode initiates a Ca^{2+} transient only when action potentials are generated (compare right and left).

Dependence of Ca^{2+} transients on electrical activity and both internal and external calcium sources

To ensure that bursts did indeed initiate Ca^{2+} transients, GnRH neurons were either treated with TTX (0.5 μM) or depolarized through the patch electrode. TTX quickly abolished firing and the occurrence of Ca^{2+} transients in all 10 GnRH neurons tested and was reversible after extensive washing (Fig. 2*a*). In a further three GnRH neurons, direct depolarization through the patch electrode was found to initiate Ca^{2+} transients only when the neuron was induced to fire action currents (Fig. 2*b*).

We evaluated the roles of both external and internal Ca^{2+} in generating Ca^{2+} transients in GnRH neurons. First, we reduced $[Ca^{2+}]$ in the extracellular space by replacing Ca^{2+} in the normal ACSF with equimolar Mg^{2+}. This resulted in a gradual run down in the amplitude and T_{rise} of Ca^{2+} transients with the area of calcium peaks decreasing from 94 ± 19 to 34 ± 33%.s ($n = 6$, $p < 0.01$, Dunn's multiple-comparison test) at 10 min (Fig. 3*a–c*) and was reversible (88 ± 38) with washout (Fig. 3*a*). The reduction and eventual loss of sharp Ca^{2+} transients correlated with a failure of the normal bursting pattern observed in GnRH neurons (Fig. 3*b*) with a 57% decrease in IBI (25.0 ± 3.9 s to 10.9 ± 1.5 s; $p < 0.01$), a threefold increase in burst duration (2.8 ± 0.3 s to 9.7 ± 2.0 s; $p < 0.05$) and an increase in spikes per burst (6.2 ± 0.5 vs 18.3 ± 3.6 spikes/burst; $p < 0.05$) (Fig. 3*c*). The role of L-type voltage-dependent calcium channels in calcium entry was examined by treating burst-firing GnRH neurons with 100 μM nifedipine. In all cases ($n = 6$), nifedipine resulted in a complete block of calcium transients and dysregulated burst firing (data not shown).

The roles of internal stores were assessed by treating GnRH neurons with 100 μM 2-APB and 30 μM CPA; antagonists at IP_3Rs and the sarcoplasmic reticulum Ca^{2+}-ATPase pump, respectively. 2-APB was found to block the calcium transients and, unexpectedly, burst firing ($n = 11$) (Fig. 3*d*). Four to 5 min after treatment of GnRH neurons ($n = 7$) with CPA, Ca^{2+} transient amplitude was suppressed and burst firing became disorganized (Fig. 3*e*); the IBI decreased significantly from 57.6 ± 12.7 s to 29.5 ± 6.2 s in the presence of CPA ($p = 0.016$) but burst duration (2.9 ± 1.0 vs 3.3 ± 1.4 s), spikes/burst (5.7 ± 1.6 vs 6.3 ± 2.2) and intraburst frequency (3.7 ± 0.7 vs 5.5 ± 2.2 Hz) were not significantly different.

These observations revealed that Ca^{2+} transients in GnRH neurons were dependent upon action potential generation and both internal and external pools of calcium; indicating that Ca^{2+} transients in GnRH neurons arise from L-type voltage-dependent membrane Ca^{2+} flux initiating Ca^{2+}-induced Ca^{2+} release from IP_3R-dependent internal stores. Importantly, the loss of this calcium amplification mechanism resulted in dysregulated burst firing suggesting that one role of the Ca^{2+} transient was to shape burst dynamics in GnRH neurons.

Modeling of Ca^{2+} dynamics in GnRH neurons

In an attempt to better understand the mechanisms underlying electrical bursting and calcium transients and their interactions in GnRH neurons, we constructed a mathematical model (Fig. 4*a*). Electrical spiking results from the interaction of Na^+ and K^+ channels while a voltage-gated Ca^{2+} channel allows for the entry of Ca^{2+} during the burst. Ca^{2+} coming in from outside then stimulates the release of additional Ca^{2+} from the ER, via IP_3-gated Ca^{2+} channels, resulting in an amplified Ca^{2+} transient. Prior studies in GnRH neurons have shown that an apamin-sensitive SK channel controls spike frequency adaptation in these cells (Kato et al., 2006; Liu and Herbison, 2008). This channel ($sI_{AHP\text{-}SK}$) was modeled to help terminate electrical bursting, while another slow Ca^{2+}-sensitive K^+ current ($sI_{AHP\text{-}UCL}$), was necessary to set the IBI in GnRH neurons. The UCL nomenclature was used due to subsequent results (*vide infra*).

Figure 4 shows simulations from the model. Electrical spiking and calcium transients are highly synchronized (Fig. 4*b*) and

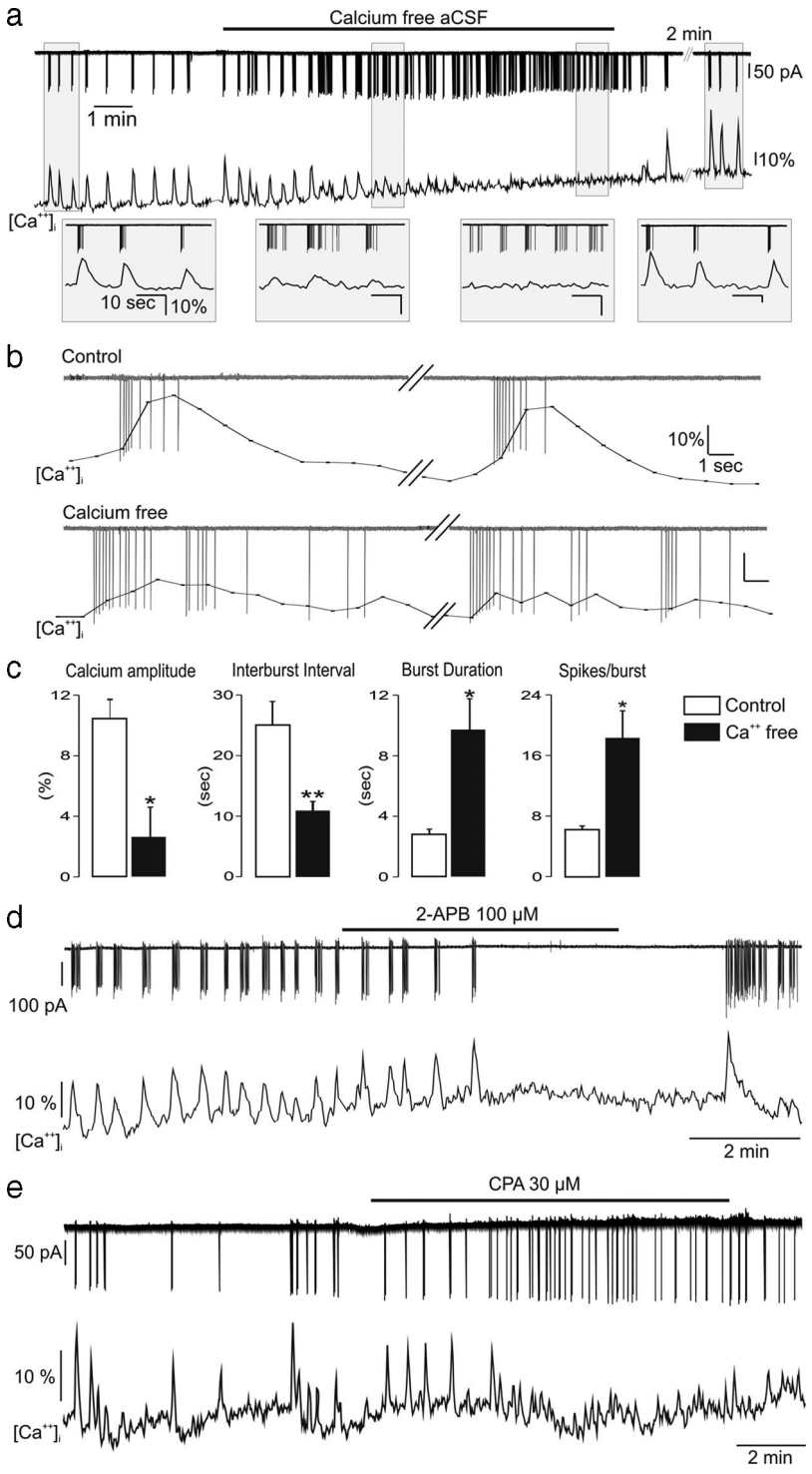

Figure 3. Calcium transients derive from both extracellular and internal sources. ***a***, Representative example showing the effect of switching to a zero [Ca^{2+}] ACSF on burst firing (top) and Ca^{2+} transients (bottom). Insets for each experimental period are shown below. ***b***, Expanded traces showing the relationship between burst firing structure and Ca^{2+} transients in control and calcium-free conditions. ***c***, Mean (±SEM) data showing the effect of calcium-free ACSF on transient amplitude, interburst interval, and burst structure. $*p < 0.05$; $**p < 0.01$; Wilcoxon signed-ranks test; $n = 6$ each group. ***d***, 2-APB, the IP_3R blocker, suppresses both Ca^{2+} transients and burst firing. ***e***, SERCA pump inhibitor CPA suppressed Ca^{2+} transient amplitude and resulted in disorganized burst firing.

eliminated by either TTX or 2-APB (compare Fig. 4*c*,*d* to Figs. 2*a*, 3*d*). Low extracellular Ca^{2+} or CPA-evoked emptying of calcium stores causes a rundown of the Ca^{2+} transients and a loss of regular bursting activity (Fig. 4*e*,*f*). Two things in particular should be noted. First, we found it was impossible to explain the entire set of experimental results without the existence of $sI_{AHP\text{-}UCL}$; the model predicted that such a channel would be found in this cell type, which turned out to be the case (Fig. 5). Furthermore, we used the model to predict the behavior that would be observed if $sI_{AHP\text{-}UCL}$ were to be blocked, a prediction that we confirmed experimentally. Second, the model provides an explanation for the puzzling experimental result that 2-APB eliminates electrical spiking, even though it is the spiking that is causing the Ca^{2+} transients. When 2-APB was modeled to inhibit only the IP_3R we obtained the same result as that seen with CPA. However, when 2-APB was modeled to inhibit the plasma membrane calcium ATPase and sarcoendoplasmic reticulum Ca^{2+}-ATPase (SERCA) pump as well as the IP_3R [as is thought to occur (Missiaen et al., 2001; Peppiatt et al., 2003)], we observed the same behavior as that seen in experimental recordings (Fig. 3*d*). This results from an increase in intracellular calcium that eliminates electrical spiking via the activation of $sI_{AHP\text{-}UCL}$ (Fig. 4*d*).

GnRH neurons exhibit long AHPs mediated by apamin- and UCL2077-sensitive channels

The modeling studies predicted that two slow Ca^{2+}-activated potassium channels were required to explain the prior correlations observed between burst firing and Ca^{2+} transients in GnRH neurons. To examine these currents and their functions in GnRH neurons, we undertook voltage- and current-clamp recordings from GFP-tagged GnRH neurons in the acute brain slice. Despite the expression of Pericam selectively in almost all GnRH neurons (Jasoni et al., 2007), the level of recordable Pericam fluorescence is low so that typically only one or two cells can be tested in any one animal. To ensure a higher chance of obtaining a tight gigaohm seal for the clamping experiments, we recorded from GFP-tagged GnRH neurons in the acute brain slice (Spergel et al., 1999). Pilot experiments undertaken in whole-cell revealed that this mode of recording was inappropriate for examining burst firing in GnRH neurons probably due to the extensive dialysis of cell milieu by the electrode; the AHP was not evident and normal burst firing including SFA was difficult to observe. As such, we used a less invasive approach using perforated patch, by which we were able to observe normal burst firing dynamics in GnRH neurons. Using a protocol established previously to fully activate the AHP in GnRH neurons (Liu and

Herbison, 2008), we confirmed the presence of a large, slowly decaying AHP (peak amplitude: 36 ± 9 pA; charge: 873 ± 322 pC; T_{decay} 22 ± 3 s, $n = 10$) (Fig. 5*a*). As the kinetics of the Ca^{2+}-dependent sI_{AHP} is sensitive to temperature (Lee et al., 2005) we performed the same perforated-patch voltage-clamp recordings at higher temperatures (32−34°C) but again found a large, slowly decaying AHP (peak amplitude: 42 ± 5 pA; charge: 437 ± 146 pC; T_{decay} 14 ± 3 s, $n = 9$, data not shown).

Previous studies in GnRH neurons have shown that 70–90% of the I_{AHP} is mediated by apamin-sensitive channels, with the identity of the remaining sI_{AHP} current unknown. The only available antagonist of the sI_{AHP} is the UCL2077 compound that has been demonstrated to be a selective blocker of the sI_{AHP} in hippocampal pyramidal cells, with minimal effects on SK channels and the mI_{AHP} (Shah et al., 2006). The relatively poor solubility of UCL2077 results in 10 μM being the highest concentration that can be used. Perforated patch voltage-clamp recordings were made from 10 GnRH neurons. In five GnRH neurons in which apamin was tested first, 300 nM apamin caused a complete block of I_{AHP} in two cells (data not shown) with the other three GnRH neurons exhibiting a partial blockade (Fig. 5*a*) with the remaining current eliminated by 10 μM UCL2077 (Fig. 5*a*). On average, apamin achieved a 72% inhibition of I_{AHP} (range 24–100%) and the combination of apamin and UCL2077 resulted in a 90% blockade of I_{AHP} in these five GnRH neurons (Fig. 5*b*). In five GnRH neurons in which UCL2077 was tested first, all cells responded and exhibited a mean 64% suppression in I_{AHP} (range 23–93%) following UCL2077 (Fig. 5*a*,*b*) and this was enhanced to a near complete 96% suppression on addition of apamin (Fig. 5*a*,*b*). Data from the eight GnRH neurons exhibiting both currents were used to determine the kinetics of the currents underlying the I_{AHP} (Fig. 5*c*). The apamin-sensitive current appeared almost instantaneously after the stimulation and reached a peak of 34 pA with a two-phase decay of 0.3 s followed by 19.0 s (total charge 352 pC) (Fig. 5*c*). In contrast, the UCL-sensitive current peaked at 14.2 s (amplitude 20 pA; total charge 634 pC) with τ_{rise} of 9.7 s and τ_{decay} of 21.0 s (Fig. 5*c*). The control vehicle (ACSF containing 0.1–0.03% dimethylsulfoxide) did not alter the I_{AHP}.

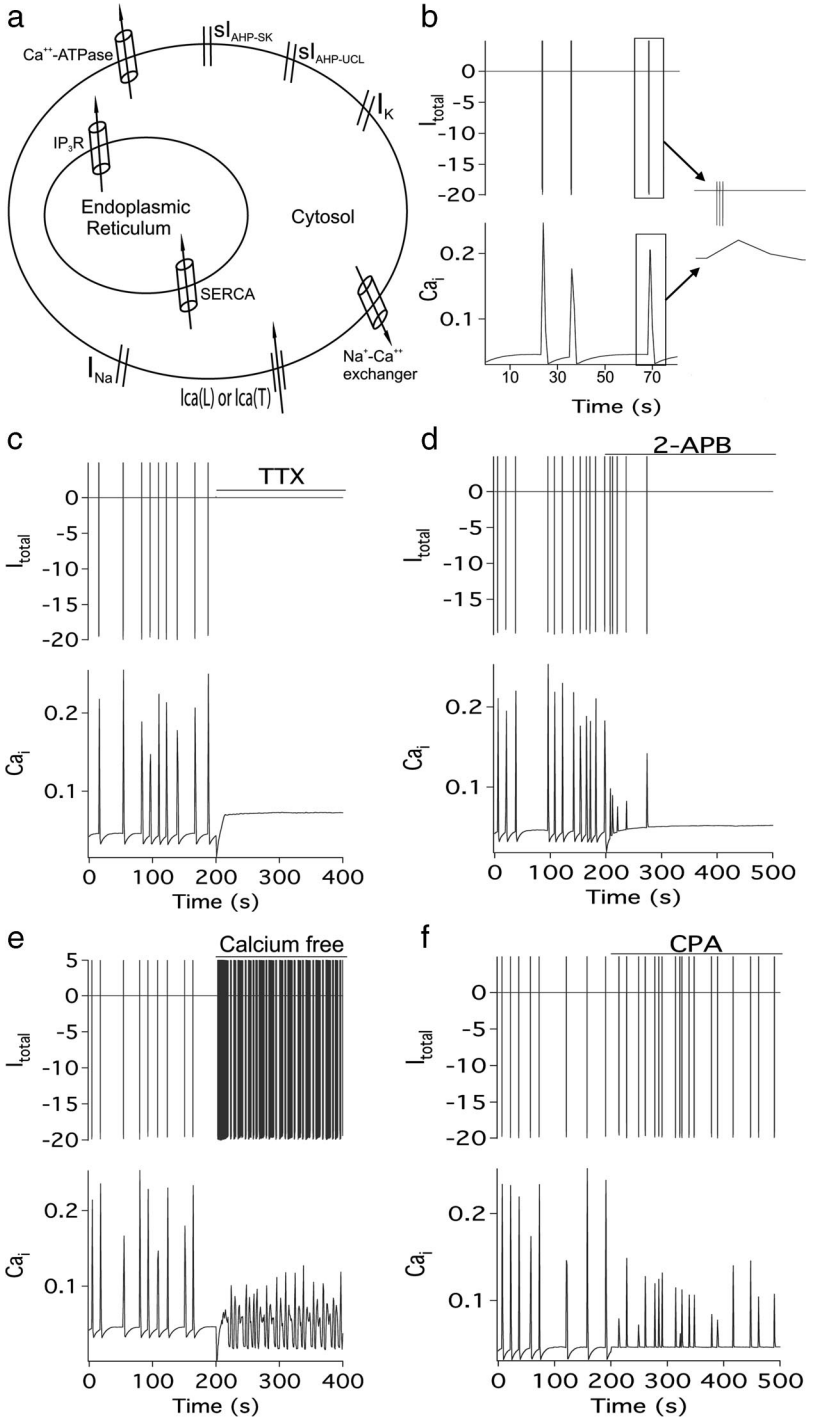

Figure 4. Mathematical model of GnRH neuron calcium and electrical behavior. ***a***, Schematic showing the key channels and pumps located in the ER and plasma membrane that comprise the model (see Materials and Methods for full description). ***b***, Baseline behavior of the model showing the relationship between burst firing (top) and $[Ca^{2+}]_i$ (bottom). The inset shows the structure of a typical burst. Subsequent panels show the effects of TTX (I_{nap} and I_{naf} set to zero) (***c***) and 2-APB ($[IP_3]$ set to zero, SERCA pump set to 30% and Ca^{2+}-ATPase set to 25%) (***d***). The precise effects of 2-APB on calcium pumps are not known, and thus these figures of 30 and 25% were chosen so as to obtain approximately the observed behavior. However, the results are not sensitive to the values chosen. ***e***, Calcium free (I_{cal} set to 40%; I_{cat} set to 30%). Experimental data indicate that calcium entry is not completely eliminated by the calcium-free solution, although the precise extent to which calcium influx is decreased is not known. Again, the figures of 40 and 30% are chosen so as to obtain approximately the correct behavior, and the model is insensitive to the exact numbers used. ***f***, Effect of CPA (SERCA set to zero) on firing and $[Ca^{2+}]_i$.

The effects of apamin and UCL2077 on the membrane excitability of 10 GnRH neurons were examined using a burst stimulation protocol [400 pA for 5 ms at 20 Hz (Chu and Moenter, 2006)] in current-clamp mode. This evoked a slow 3.2 ± 1.9 mV AHP (τ_{drop} = 1.8 ± 0.5 s; $\tau_{recovery}$ = 16.2 ± 5.4 s) (Fig. 5*d*). The effects of 300 nM apamin to suppress the AHP were variable between cells but, as a group, had no significant effect (60 ± 38% of

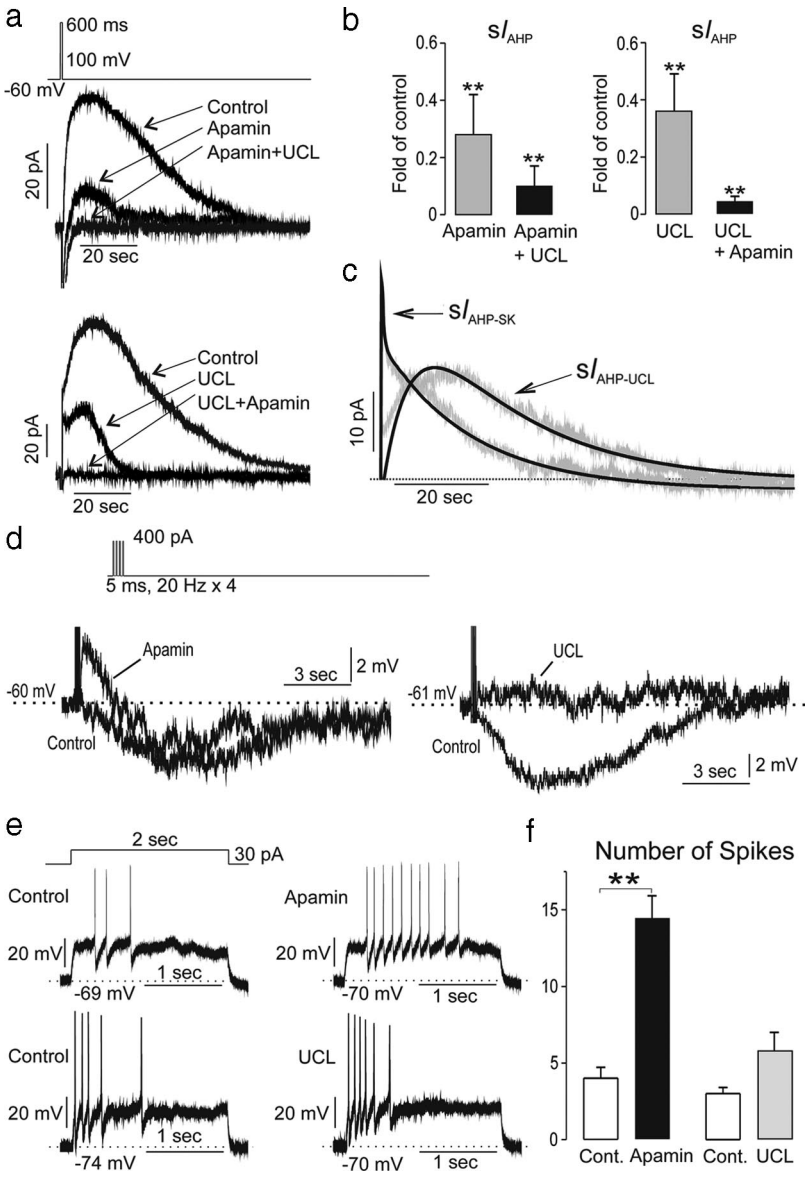

Figure 5. The AHP in GnRH neurons is mediated by two sI_{AHP}s. ***a***, Perforated-patch, voltage-clamp traces from two GnRH neurons showing the evoked I_{AHP} and its modulation by 300 nM apamin and 10 μM UCL2077. The top cell received apamin then UCL2077 while the bottom cell received the blockers in the reverse order. Each curve is the mean of two repetitions. ***b***, Group (mean ± SEM) data showing fold decrease in I_{AHP} by apamin alone and then combined with UCL2077 (left) or UCL2077 alone and combined with apamin (right; $^{**}p < 0.01$; Dunnett's multiple-comparison test vs control; $n = 5$ each group). ***c***, Derived dynamics of apamin- and UCL2077-sensitive currents generated by averaging subtracted curves from individual cells ($n = 8$). The kinetics of both apamin-sensitive and UCL2077-sensitive currents were well described by exponential rising and decay functions (black lines; with $r = 0.89$ and $r = 0.87$, respectively). ***d***, Effects of apamin or UCL2077 on evoked (400 pA for 5 ms at 20 Hz) AHP measured in current-clamp mode. Apamin evoked a large afterdepolarization potential and variable ($p > 0.05$) suppressive effects on the AHP. UCL blocked the AHP only. ***e***, Effect of apamin (top) and UCL2077 (bottom) on intraburst dynamics induced by 30 pA current for 2 s. ***f***, Group data (mean ± SEM, $n = 5$ each) showing effects of apamin and UCL2077 on number of spikes per burst. $^{**}p < 0.01$; Wilcoxon signed-ranks test.

the control, $p = 0.37$, $n = 5$) (Fig. 5*d*). This was likely due to the ability of apamin to allow the appearance of a prominent slow afterdepolarizing potential (sADP) in GnRH neurons (4.9 ± 2.3 mV, $n = 5$) (Fig. 5*d*) (Chu and Moenter, 2006; Liu and Herbison, 2008) that counteracts the ability to observe any suppressive effect of apamin on the AHP. This possibility was confirmed by showing a significant decrease in sAHP by apamin when the sADP was more strongly suppressed by injecting a higher level of current (1500 pA for 10 ms at 20 Hz). In the voltage-clamp mode, sI_{AHP} was significantly suppressed from 146.9 ± 22.8 pA · s to 56.0 ± 19.3 pA · s ($p = 0.008$, $n = 8$). As a consequence, the AHP was significantly depressed from −73 ± 21 mV · s to −0.1 ± 15.8 mV · s ($p = 0.007$, $n = 8$) in the current-clamp mode. In contrast to apamin, 10 μM UCL2077 significantly reduced the AHP to 22 ± 10% of the control ($p = 0.03$, $n = 5$) (Fig. 5*d*) but had no effect on ADP magnitude.

These observations show that the long-lasting AHP in GnRH neurons is generated by two pharmacologically and kinetically distinct sI_{AHP} currents.

The two sAHP currents in GnRH neurons regulate different aspects of burst firing

Testing the effects of apamin ($sI_{AHP\text{-}SK}$ set to zero) and UCL2077 [$sI_{AHP\text{-}UCL}$ set to 50%; 10 μM UCL2077 is reported to be the IC_{50} for blocking the sI_{AHP} in hippocampal cells (Shah et al., 2006)] in the mathematical model of Ca^{2+} dynamics in GnRH neurons predicted that apamin would slow burst firing and reduce SFA while UCL2077 would decreased the IBI and have little effect upon intraburst firing dynamics (data not shown).

Current-clamp recordings were undertaken to evaluate the effects of apamin and UCL2077 on evoked and endogenous SFA in GnRH-GFP neurons. As shown previously in GnRH neurons (Liu and Herbison, 2008), a 30 pA current injection protocol for 2 s initiates a burst of action potentials exhibiting strong SFA (Fig. 5*e*). Treatment with 300 nM apamin resulted in threefold increase in spike number and clear reduction in SFA ($n = 5$) (Fig. 5*e*,*f*). In contrast, 10 μM UCL2077 (10 μM) had no significant effect on the number of spikes or SFA (Fig. 5*e*,*f*). To examine the effects of apamin and UCL2077 on the patterning of endogenous bursting and calcium dynamics in GnRH neurons, noninvasive dual electrical-Ca^{2+} recordings were undertaken in GnRH-Pericam mice. Apamin significantly slowed the rate of burst induction (Fig. 6*a*,*b*) (9.6 ± 2.3 bursts vs 5.0 ± 1.2 bursts, $p = 0.04$, $n = 7$) and exhibited the same effects on intraburst dynamics as seen in evoked responses (Fig. 5*f*). Apamin induced more spikes per burst with loss of SFA, and a modest increase in intraburst frequency (Fig. 6*b*). As indicated by our previous correlational analysis, Ca^{2+} transients (amplitude, T_{rise}, or T_{decay}) were not altered significantly by changes in burst firing induced by apamin. In contrast to apamin, treatment with UCL2077 resulted in a marked shortening of IBI (5.3 ± 1.2 bursts/10 min in control vs 11.3 ± 2.8 bursts/10 min with UCL2077; $p = 0.035$, $n = 6$) (Fig. 6*c*,*d*) with no significant effects on intraburst spiking dynamics (burst duration, spikes/burst, intraburst frequency) (Fig. 6*d*). As predicted by the relationship determined above be-

tween IBI and transient amplitude (Fig. 1*h*,*i*), the markedly decreased IBI in the presence of UCL2077 was associated with a significant decrease of the amplitude of calcium transients (13.5 ± 1.3% baseline to 9.0 ± 1.3% baseline, $n = 7$, $p = 0.015$).

Discussion

These studies demonstrate that the slow Ca^{2+} transients observed in adult GnRH neurons represent a faithful signature of their burst firing. Initiated by voltage-dependent Ca^{2+} entry across the plasma membrane and amplified by Ca^{2+}-induced Ca^{2+} release from internal stores, the ~10 s duration Ca^{2+} transients greatly outlast the ~2-s-long action potential bursts of GnRH neurons. While such Ca^{2+} transients will likely have multiple roles within the GnRH neuron, we show here that one important task is to confine burst firing dynamics to typically five spikes per burst with an IBI of 15–20 s. This is achieved by the Ca^{2+} transient regulating two pharmacologically distinct channels underlying the sAHP of GnRH neurons; an apamin-sensitive channel controlling both intraburst and interburst dynamics and a UCL2077-sensitive channel controlling interburst dynamics.

The broad Ca^{2+} transient in GnRH neurons is initiated by voltage-dependent calcium entry across the membrane. Spontaneous transients were (1) abolished by tetrodotoxin, (2) initiated by 20 mM potassium, and (3) evoked by direct depolarization of the cell only when action potentials were generated. Calcium entry through voltage-gated calcium channels would, however, be too brief to explain the ~3 s rise kinetics of the observed Ca^{2+} transient. It was not surprising, therefore, to find that both 2-APB and CPA suppressed Ca^{2+} transients in GnRH neurons indicating an important role for intracellular stores. Together these observations indicate that IP_3R-dependent Ca^{2+}-induced Ca^{2+} release is used to amplify the brief Ca^{2+} membrane flux into a prolonged Ca^{2+} transient. Specific voltage-dependent Ca^{2+} channels are associated with the activation of different Ca^{2+}-activated potassium channels in striatal neurons (Goldberg and Wilson, 2005) and compatible with this, we found that L-type calcium channels are responsible for store-amplified calcium influx in GnRH neurons. Interestingly, the amplitude and kinetics of individual Ca^{2+} transients were relatively homogeneous and found to be independent of most burst parameters including spike number ($r = 0.10$); indeed, the occasional burst comprised of only one spike could generate a normal-sized Ca^{2+} transient equivalent to that of a five-spike burst. This suggests that stores release a certain "quanta" of Ca^{2+} in response to a range of plasma membrane Ca^{2+} influx. However, as has been noted previously (Power and Sah, 2005), store release can fail if activated with insufficient time for refilling. This is likely occurring in GnRH neurons, for which an IBI of <15 s resulted in the subsequent Ca^{2+} transient having a reduced amplitude. Thus, as long as individual bursts are spaced sufficiently, spontaneous burst firing in GnRH neurons results in very robust, prolonged Ca^{2+} transients.

Roles for SK, KCNQ, and molecularly unidentified Ca^{2+}-actvated potassium channels have being described for generating the AHP in neurons (Sah and Faber, 2002; Gu et al., 2005; Pedarzani and Stocker, 2008; Tzingounis and Nicoll, 2008). In nearly all neurons examined, the SK channel is implicated in mediating the majority of the mAHP with little direct role in the

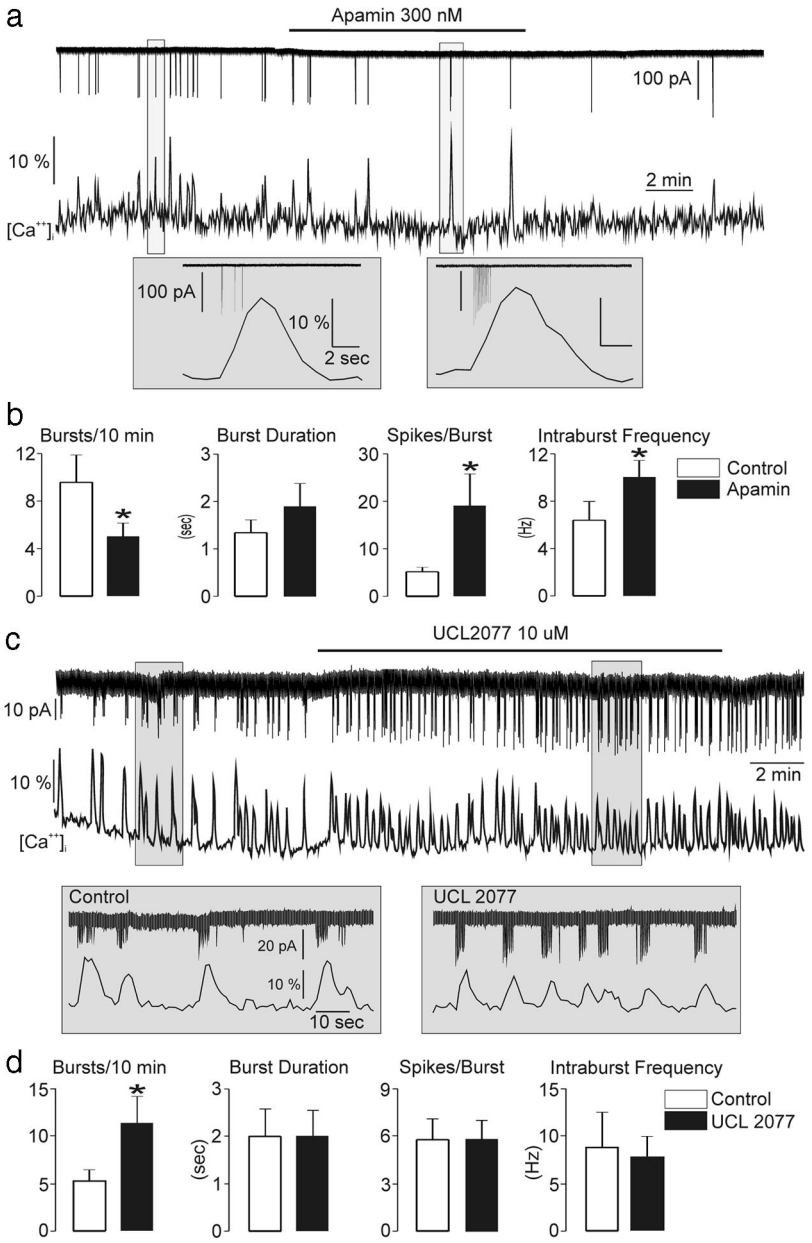

Figure 6. The apamin- and UCL2077-sensitive currents differentially modulate GnRH neuron burst firing dynamics. ***a***, Representative trace showing the effect of apamin on burst firing and Ca^{2+} transients. Insets for each experimental period are shown below. ***b***, Mean (±SEM) data showing effects of apamin on burst dynamics in GnRH neurons (*$p < 0.05$; Wilcoxon signed-ranks test; $n = 7$). ***c***, Representative trace showing the effect of UCL2077 on burst firing and Ca^{2+} transients. Insets for each experimental period are shown below. ***d***, Mean (±SEM) data showing effects of UCL2077 on burst firing dynamics in GnRH neurons. *$p < 0.05$; Wilcoxon signed-ranks test; $n = 7$.

sAHP (Bond et al., 2004; Pedarzani and Stocker, 2008). The one exception to this is the GnRH neuron, for which the apamin-sensitive current persists for several seconds in both mice and rats (Kato et al., 2006; Spergel, 2007; Liu and Herbison, 2008). As GnRH neurons express mRNA for all three SK channels (Bosch et al., 2002; Kato et al., 2006) it is very likely that SK channels underlie the apamin-sensitive currents ($sI_{AHP\text{-}SK}$) in these cells. However, it is unclear why the $sI_{AHP\text{-}SK}$ decay is so prolonged in these cells and best modeled by a two phase dynamic comprised of a rapid (~0.3 s) and a long decay (~19 s). The initial decay is compatible with the mAHP current mediated by the SK channel recorded in other neurons, but the latter slow phase appears unique to GnRH neurons. In other neurons, SK channel activation and decay tends to faithfully follow the cytosolic $[Ca^{2+}]_i$ resulting from voltage-dependent Ca^{2+} entry (Sah and Faber, 2002). This remains the situation even when IP_3R-dependent stores are involved in generating Ca^{2+} transients regulating SK currents (Yamada et al., 2004; Gulledge and Stuart, 2005). This would not explain the situation fully in GnRH neurons, however, in which the long ~8 s Ca^{2+} transients are only lasting for approximately half the duration of the $sI_{AHP\text{-}SK}$ current (~20 s). The reasons for such prolonged currents in GnRH neurons are not known and may result, in part, from the existence of membrane-associated Ca^{2+} microdomains, unusual binding affinities of Ca^{2+} to calcium sensors and buffers (Sah and Clements, 1999; Tzingounis et al., 2007) and/or unique patterns of kinase-dependent channel phosphorylation (Maingret et al., 2008).

Prompted by the curious results we obtained with 2-APB inhibiting burst firing, we initiated a mathematical modeling exercise to help understand the likely complex Ca^{2+} regulation of GnRH neuron electrical excitability. In undertaking this exercise, it became readily apparent that our initial results could not be explained solely by modeling known or even slow SK channel function and that an independent, longer duration calcium-activated channel suppressing burst onset was required. This suggested the presence of the unidentified Ca^{2+}-activated potassium channel underlying the sAHP as has been described in several cell types (Sah and Faber, 2002). The UCL2077 compound has been demonstrated to be a selective blocker of the sAHP in hippocampal pyramidal cells, with minimal effects on SK channels and the mI_{AHP} (Shah et al., 2006). We find here that 10 μM UCL2077 is extremely effective in blocking nearly all of the remaining apamin-insensitive component of the sAHP current in GnRH neurons. In hippocampal neurons, 10 μM UCL2077 (the highest concentration that can be used *in vitro*) is thought to be the IC_{50} for the sAHP current (Shah et al., 2006) but it would appear to be much more effective here in GnRH neurons. While it remains possible that UCL2077 could have a small impact upon SK channels (Shah et al., 2006), this was not apparent in the present studies as apamin and UCL2077 exhibited very different, and even opposite, effects upon the sADP, sI_{AHP} amplitude, SFA and GnRH neuron burst firing. Such observations indicate that UCL2077 is not modulating SK channel activity and demonstrate distinct roles for $sI_{AHP\text{-}SK}$ and $sI_{AHP\text{-}UCL}$ in regulating GnRH neuron excitability. The UCL2077-sensitive current was found to have a slow onset ($\tau_{rise} = 9.7$ s) and very slow single exponential decay ($\tau_{decay} = 21$ s). As for $sI_{AHP\text{-}SK}$, the duration of $sI_{AHP\text{-}UCL}$ in GnRH neurons is very prolonged compared with sAHP and $sI_{AHP\text{-}UCL}$ reported in other neuronal phenotypes and this may reflect unique Ca^{2+} handling in GnRH neurons or even the expression of particular subtypes of the as yet uncharacterized channels underlying the sI_{AHP}.

Treatment with apamin revealed that $sI_{AHP\text{-}SK}$ is responsible for SFA adaptation in GnRH neurons and normally restricts GnRH neuron bursts to ~5 spikes/burst. In contrast, $sI_{AHP\text{-}UCL}$ had little or no effect upon burst structure but exerted a powerful restraining influence upon the timing of bursts. Recent studies have highlighted likely interactions between SK and sI_{AHP} channels in the regulation of neuronal firing in the striatum and amygdala (Power and Sah, 2008; Goldberg et al., 2009). Although we find some evidence for interaction in terms of regulating IBI, burst dynamics are clearly dependent on only $sI_{AHP\text{-}SK}$. This likely to be due to the activation kinetics of $sI_{AHP\text{-}UCL}$ (τ_{rise} ~10 s) being too slow to contribute to the structure of bursts that only last ~2 s.

As with other neuroendocrine output neurons, it seems likely that the bursting behavior of GnRH neurons is key for pulsatile GnRH secretion (Leng and Brown, 1997; Moenter et al., 2003; Herbison, 2006) but the mechanisms responsible for burst firing had not been delineated until now. We show here that a critical feature for burst firing by GnRH neurons is their ability to exhibit prolonged Ca^{2+} transients that act, in turn, to control very slow I_{AHP}s that regulate intraburst and interburst properties. It is interesting to note that magnocellular oxytocin and vasopressin neurons can exhibit somewhat similar bursting behaviors to GnRH neurons but do not exhibit prolonged calcium transients or use calcium-dependent potassium channels in the same manner (Li and Hatton, 1997; Ghamari-Langroudi and Bourque, 2004; Teruyama and Armstrong, 2005). The dynamics of Ca^{2+} transients in GnRH neurons are unique in the mature nervous system as is the existence of a very slow AHP generated by two sI_{AHP}s in these cells. That one of these currents is apamin sensitive is surprising given prior data indicating that SK channels underlie currents with a duration of 100 ms (Pedarzani and Stocker, 2008), rather than many seconds.

While the ionic mechanism elucidated here is demonstrated to constrain GnRH neuron burst firing to ~5 action potentials per burst every 20 s, it remains that the initiating mechanism for a burst is unknown. The GnRH neurons exhibit a slow ADP (Chu and Moenter, 2006) that may contribute, as might hyperpolarization-activated channels (Kelly and Wagner, 2002). Indeed, one plausible scenario underpinning GnRH neuron burst firing would be that calcium-activated sI_{AHP}s act to regulate the balance between sAHPs and sADPs (Brown and Bourque, 2006) responsible for initiating the next burst of firing. The present findings help define the ionic basis for burst firing in the GnRH neurons and outline a unique calcium sI_{AHP} mechanism for achieving this.

References

Berridge MJ (1998) Neuronal calcium signaling. Neuron 21:13–26.

Bond CT, Herson PS, Strassmaier T, Hammond R, Stackman R, Maylie J, Adelman JP (2004) Small conductance Ca^{2+}-activated K^+ channel knock-out mice reveal the identity of calcium-dependent afterhyperpolarization currents. J Neurosci 24:5301–5306.

Bosch MA, Kelly MJ, Rønnekleiv OK (2002) Distribution, neuronal colocalization, and 17beta-E2 modulation of small conductance calcium-activated K(+) channel (SK3) mRNA in the guinea pig brain. Endocrinology 143:1097–1107.

Brown CH, Bourque CW (2006) Mechanisms of rhythmogenesis: insights from hypothalamic vasopressin neurons. Trends Neurosci 29:108–115.

Chu Z, Moenter SM (2006) Physiologic regulation of a tetrodotoxin-sensitive sodium influx that mediates a slow afterdepolarization potential in gonadotropin-releasing hormone neurons: possible implications for the central regulation of fertility. J Neurosci 26:11961–11973.

Ghamari-Langroudi M, Bourque CW (2004) Muscarinic receptor modulation of slow afterhyperpolarization and phasic firing in rat supraoptic nucleus neurons. J Neurosci 24:7718–7726.

Goldberg JA, Wilson CJ (2005) Control of spontaneous firing patterns by the selective coupling of calcium currents to calcium-activated potassium currents in striatal cholinergic interneurons. J Neurosci 25:10230–10238.

Goldberg JA, Teagarden MA, Foehring RC, Wilson CJ (2009) Nonequilibrium calcium dynamics regulate the autonomous firing pattern of rat striatal cholinergic interneurons. J Neurosci 29:8396–8407.

Gu N, Vervaeke K, Hu H, Storm JF (2005) Kv7/KCNQ/M and HCN/h, but not KCa2/SK channels, contribute to the somatic medium after-hyperpolarization and excitability control in CA1 hippocampal pyramidal cells. J Physiol 566:689–715.

Gulledge AT, Stuart GJ (2005) Cholinergic inhibition of neocortical pyramidal neurons. J Neurosci 25:10308–10320.

Han SK, Gottsch ML, Lee KJ, Popa SM, Smith JT, Jakawich SK, Clifton DK, Steiner RA, Herbison AE (2005) Activation of gonadotropin-releasing hormone (GnRH) neurons by kisspeptin as a neuroendocrine switch for the onset of puberty. J Neurosci 25:11349–11356.

Herbison AE (2006) Physiology of the GnRH neuronal network. In: Knobil and Neill's physiology of reproduction, Ed 3 (Neill JD, ed), pp 1415–1482. San Diego: Academic.

Jasoni CL, Todman MG, Strumia MM, Herbison AE (2007) Cell type-specific expression of a genetically encoded calcium indicator reveals intrinsic calcium oscillations in adult gonadotropin-releasing hormone neurons. J Neurosci 27:860–867.

Kato M, Tanaka N, Usui S, Sakuma Y (2006) The SK channel blocker apamin inhibits slow afterhyperpolarization currents in rat gonadotropin-releasing hormone neurones. J Physiol 574:431–442.

Keener J, Sneyd J (2008) Mathematical physiology, Ed 2. New York: Springer.

Kelly MJ, Wagner EJ (2002) GnRH neurons and episodic bursting activity. Trends Endocrinol Metab 13:409–410.

LeBeau AP, Van Goor F, Stojilkovic SS, Sherman A (2000) Modeling of membrane excitability in gonadotropin-releasing hormone-secreting hypothalamic neurons regulated by Ca^{2+}-mobilizing and adenylyl cyclase-coupled receptors. J Neurosci 20:9290–9297.

Lee JC, Callaway JC, Foehring RC (2005) Effects of temperature on calcium transients and Ca^{2+}-dependent afterhyperpolarizations in neocortical pyramidal neurons. J Neurophysiol 93:2012–2020.

Leng G, Brown D (1997) The origins and significance of pulsatility in hormone secretion from the pituitary. J Neuroendocrinol 9:493–513.

Li YX, Rinzel J, Keizer J, Stojilković SS (1994) Calcium oscillations in pituitary gonadotrophs: comparison of experiment and theory. Proc Natl Acad Sci U S A 91:58–62.

Li Z, Hatton GI (1997) Ca^{2+} release from internal stores: role in generating depolarizing after-potentials in rat supraoptic neurones. J Physiol 498:339–350.

Liu X, Herbison AE (2008) Small-conductance calcium-activated potassium channels control excitability and firing dynamics in gonadotropin-releasing hormone (GnRH) neurons. Endocrinology 149:3598–3604.

Maingret F, Coste B, Hao J, Giamarchi A, Allen D, Crest M, Litchfield DW, Adelman JP, Delmas P (2008) Neurotransmitter modulation of small-conductance Ca^{2+}-activated K^+ channels by regulation of Ca^{2+} gating. Neuron 59:439–449.

Maylie J, Bond CT, Herson PS, Lee WS, Adelman JP (2004) Small conductance Ca^{2+}-activated K^+ channels and calmodulin. J Physiol 554:255–261.

Missiaen L, Callewaert G, De Smedt H, Parys JB (2001) 2-Aminoethoxydiphenyl borate affects the inositol 1,4,5-trisphosphate receptor, the intracellular Ca^{2+} pump and the non-specific Ca^{2+} leak from the non-mitochondrial Ca^{2+} stores in permeabilized A7r5 cells. Cell Calcium 29:111–116.

Moenter SM, DeFazio AR, Pitts GR, Nunemaker CS (2003) Mechanisms underlying episodic gonadotropin-releasing hormone secretion. Front Neuroendocrinol 24:79–93.

Nagai T, Sawano A, Park ES, Miyawaki A (2001) Circularly permuted green fluorescent proteins engineered to sense Ca^{2+}. Proc Natl Acad Sci U S A 98:3197–3202.

Nicoll RA (1988) The coupling of neurotransmitter receptors to ion channels in the brain. Science 241:545–551.

Pedarzani P, Stocker M (2008) Molecular and cellular basis of small- and intermediate-conductance, calcium-activated potassium channel function in the brain. Cell Mol Life Sci 65:3196–3217.

Peppiatt CM, Collins TJ, Mackenzie L, Conway SJ, Holmes AB, Bootman MD, Berridge MJ, Seo JT, Roderick HL (2003) 2-Aminoethoxydiphenyl borate (2-APB) antagonises inositol 1,4,5-trisphosphate-induced calcium release, inhibits calcium pumps and has a use-dependent and slowly reversible action on store-operated calcium entry channels. Cell Calcium 34:97–108.

Perkins KL (2006) Cell-attached voltage-clamp and current-clamp recording and stimulation techniques in brain slices. J Neurosci Methods 154:1–18.

Power JM, Sah P (2005) Intracellular calcium store filling by an L-type calcium current in the basolateral amygdala at subthreshold membrane potentials. J Physiol 562:439–453.

Power JM, Sah P (2008) Competition between calcium-activated K^+ channels determines cholinergic action on firing properties of basolateral amygdala projection neurons. J Neurosci 28:3209–3220.

Roberts CB, O'Boyle MP, Suter KJ (2009) Dendrites determine the contribution of after depolarization potentials (ADPs) to generation of repetitive action potentials in hypothalamic gonadotropin releasing-hormone (GnRH) neurons. J Comput Neurosci 26:39–53.

Romanò N, Lee K, Abrahám IM, Jasoni CL, Herbison AE (2008) Nonclassical estrogen modulation of presynaptic GABA terminals modulates calcium dynamics in gonadotropin-releasing hormone neurons. Endocrinology 149:5335–5344.

Sah P, Clements JD (1999) Photolytic manipulation of $[Ca2^+]_i$ reveals slow kinetics of potassium channels underlying the afterhyperpolarization in hippocampal pyramidal neurons. J Neurosci 19:3657–3664.

Sah P, Faber ES (2002) Channels underlying neuronal calcium-activated potassium currents. Prog Neurobiol 66:345–353.

Salkoff L, Butler A, Ferreira G, Santi C, Wei A (2006) High-conductance potassium channels of the SLO family. Nat Rev Neurosci 7:921–931.

Shah MM, Javadzadeh-Tabatabaie M, Benton DC, Ganellin CR, Haylett DG (2006) Enhancement of hippocampal pyramidal cell excitability by the novel selective slow-afterhyperpolarization channel blocker 3-(triphenylmethylaminomethyl)pyridine (UCL2077). Mol Pharmacol 70:1494–1502.

Sim JA, Skynner MJ, Herbison AE (2001) Heterogeneity in the basic membrane properties of postnatal gonadotropin-releasing hormone neurons in the mouse. J Neurosci 21:1067–1075.

Sneyd J, Dufour JF (2002) A dynamic model of the type-2 inositol trisphosphate receptor. Proc Natl Acad Sci U S A 99:2398–2403.

Spergel DJ (2007) Calcium and small-conductance calcium-activated potassium channels in gonadotropin-releasing hormone neurons before, during, and after puberty. Endocrinology 148:2383–2390.

Spergel DJ, Krüth U, Hanley DF, Sprengel R, Seeburg PH (1999) GABA- and glutamate-activated channels in green fluorescent protein-tagged gonadotropin-releasing hormone neurons in transgenic mice. J Neurosci 19:2037–2050.

Teruyama R, Armstrong WE (2005) Enhancement of calcium-dependent afterpotentials in oxytocin neurons of the rat supraoptic nucleus during lactation. J Physiol 566:505–518.

Tzingounis AV, Nicoll RA (2008) Contribution of KCNQ2 and KCNQ3 to the medium and slow afterhyperpolarization currents. Proc Natl Acad Sci U S A 105:19974–19979.

Tzingounis AV, Kobayashi M, Takamatsu K, Nicoll RA (2007) Hippocalcin gates the calcium activation of the slow afterhyperpolarization in hippocampal pyramidal cells. Neuron 53:487–493.

Vogalis F, Storm JF, Lancaster B (2003) SK channels and the varieties of slow after-hyperpolarizations in neurons. Eur J Neurosci 18:3155–3166.

Wilson CJ, Goldberg JA (2006) Origin of the slow afterhyperpolarization and slow rhythmic bursting in striatal cholinergic interneurons. J Neurophysiol 95:196–204.

Yamada S, Takechi H, Kanchiku I, Kita T, Kato N (2004) Small-conductance Ca^{2+}-dependent K^+ channels are the target of spike-induced Ca^{2+} release in a feedback regulation of pyramidal cell excitability. J Neurophysiol 91:2322–2329.